Journal of Molecular Graphics and Modelling 53 (2014) 1–12

Contents lists available at ScienceDirect

Journal of Molecular Graphics and Modelling

journal homepage: www.elsevier.com/locate/JMGM

In silico screening and study of novel ERK2 inhibitors using 3D QSAR, docking and molecular dynamics

Sofiene Larif[a,*], Chaker Ben Salem[b], Houssem Hmouda[b], Kamel Bouraoui[b]

[a] Metabolic Biophysics and Applied Pharmacology Laboratory, Department of Biophysics, Faculty of Medicine of Sousse, 4002 Sousse, Tunisia
[b] Department of Clinical Pharmacology, Faculty of Medicine of Sousse, 4002 Sousse, Tunisia

ARTICLE INFO

Article history:
Accepted 2 July 2014
Available online 10 July 2014

Keywords:
ERK2
3D QSAR pharmacophore
HypoGen
Molecular docking
LigandFit
Molecular dynamics

ABSTRACT

ERK2 is a dual specificity protein kinase, part of the Ras/Raf/MEK/ERK signal transduction cascade. It forms an interesting target for inhibition based on its relationship with cell proliferation and oncogenesis. A 3D QSAR pharmacophore model (Hypo1) with high correlation ($r = 0.938$) was developed for ERK2 ATP site on the basis of experimentally known inhibitors. The model included three hydrogen bonds, and one hydrophobic site. Assessment of Hypo1 through Fisher randomization, cost analysis, leave one out method and decoy test suggested that the model can reliably detect ERK2 inhibitors. Hypo1 has been used for virtual screening of potential inhibitors from ZINC, Drug Bank, NCI, Maybridge and Chembank databases. Using Hypo1 as a query, databases have been interrogated for compounds who meet the pharmacophore features. The resulting hit compounds were subject to docking and analysis. Docking and molecular dynamics analysis showed that in order to achieve a higher potency compounds have to interact with catalytic site, glycine rich loop, Hinge region, Gatekeeper region and ATP site entrance residues. We also identified catalytic site and Glycine rich loop as important regions to bind by molecules for better potency and selectivity.

1. Introduction

In the last decade, protein kinases have received a large attention from the scientific and pharmaceutical community in an attempt to develop small molecules inhibitors [1]. Interest in this superfamily of proteins is due to its crucial role in cell regulation. Indeed, normal cells sense their external environment through cascades of kinases reactions taking the activation of a cell surface receptor as their initial triggering event. The type of the activated cascade(s) mediates the cell behavior of proliferation, growth and interaction with external signal or even apoptosis. Because Protein kinases exist in almost every cell, they are involved in diverse physiological roles such as inflammation, immunity and development. Disruption of kinases pathways can alter the cell signal transduction as in cardiac pathology [2], Alzheimer's disease [3] and hematologic malignancies such as acute leukemia [4,5].

Ras/Raf/MEK/ERK signal transduction cascade is one of multiple pathways involved in several malignancies. The alteration of this pathway has been reported in cancers of lung [6], ovary [7], kidney [8], colon [9], and pancreas [10]. Oncogenesis can be related to kinases receptor's over-expression or mutations [11]. In order to produce therapeutic anti-tumoral agent's, ERK protein kinases can be potentially a good target for inhibition [12].

ERK kinases are Dual-specificity kinases requiring phosphorylation of both serine and threonine residues for catalytic activation. ERK2 is one of the best targets for inhibition within the ERK kinase subgroup since this protein can have cell pro-proliferative effects [13]. Also, since ERK2 kinase belongs to the small group of dual-specificity kinases, this property leads to a higher specificity and an increased catalytic activity that can be as high as 600,000 folds [14]. Moreover, the ERK2 forms a convergence point of a large number of upstream pathways which offer the opportunity for a strong inhibition.

Because of that, the discovery of ERK2 inhibitors can be important to a number of pathologies especially tumoral proliferations. In this study, we focused on ERK2 rational drug design to find new leads/scaffolds which can be able to have a potent inhibitory effect. A 3D pharmacophore model capable of distinguishing potent inhibitors has been built using known ERK2 inhibitors. The pharmacophore model have been used as a 3D request to find a number of

* Corresponding author at: Metabolic Biophysics and Applied Pharmacology Laboratory, Department of Biophysics, Faculty of Medicine of Sousse, Avenue Mohamed Karoui, 4002 Sousse, Tunisia. Tel.: +216 92 059 195; fax: +216 73 224 899.
E-mail address: Larifsofiene@gmail.com (S. Larif).

http://dx.doi.org/10.1016/j.jmgm.2014.07.001
1093-3263/

molecules that have been subjects to docking and ranking followed by a molecular dynamics (MD) analysis of ligand–protein complex stability.

2. Material and methods

2.1. Data training and test set preparation

2.1.1. Dataset

The generation of a pharmacophore model should satisfy certain rules such as: using a minimum of 18 compounds with different structures and activity range with at least four order magnitudes. For this study, a selected set of 39 compounds with known activities has been taken from literature [15,16]. Inhibitory data was obtained by biochemical assay with activity value K_i ranged between 2 nM and 2.3 μM with respect to pharmacophore generation rules, used compounds have been chosen to be the most actives against the ERK2 target with the highest possible selectivity. Dataset was divided randomly into training and test set with 70% of molecules in the training set (27 compounds) and 30% in the test set (12 compounds). The training set was used to generate the 3D-QSAR model and build the pharmacophore query while the test set was used to validate the model.

2.1.2. Ligand preparation

In order to obtain a reliable pharmacophore model, the set of active compounds should be prepared before the model training. The two-dimensional (2D) dataset chemical structures were sketched using Accelrys draw 4.1. Sketching was followed by hydrogen addition, conversion into 3D structures, PH based ionization and charge neutralization. This preparation includes 3D structure generation followed by sampling of the conformational space to obtain representative 3D conformations. A maximum of 255 diverse conformers were generated with an energy threshold of 15 kcal. Energy minimization was performed using the Chemistry at Harvard Macromolecular Mechanics (CHARMM) forcefield. The search for local minima was carried by a Steepest Descent minimization, followed by Conjugate Gradient minimization. The prepared structures were used to generate hypothesis with Discovery Studio.

2.2. Pharmacophore generation

3D-QSAR techniques have been used with success as an alternative to the free energies calculation methods which are costly in computational time and resources. A number of papers highlight the acceptable performance of using 3D-QSAR/pharmacophore based techniques compared to docking [17–19]. 3D-QSAR can be a reliable technique in term of providing a relationship between 3 dimensional structure and biological activity. In the case where structures of both ligand and receptor are present, a series of ligand–receptor complexes can help quantify energy of interaction by the mean of computational mechanics. From this interaction data a 3D-QSAR model can be obtained by decomposing interaction energy per residue into electrostatic and van der walls components followed by a partial least square (PLS) regression analysis. Another approach is based on the knowledge of only ligands structures and theirs activities. This method can be used for the build of a 3D-QSAR model from an alignment of the training compounds. All superimposed molecules will be placed in the center of a lattice grid where both steric and electrostatic energy fields are calculated by the mean of 'probes'. Using PLS, influence of each chemical features on biological activity are quantified and a linear correlation equation can be generated. This equation can be used to predict activities of unknown molecules.

The pharmacophore theory was described the first time by Kier in 1967 and used in a series of papers published from 1967 to 1971 [20,21]. A common pharmacophore hypothesis is a shared spatial arrangement of multiple chemical features between two or more active compounds. This hypothesis was proposed as an explanation of some selected ligand–receptor interactions. The prepared 27 compounds of the training set were submitted to the HypoGen module for pharmacophore generation. The hydrogen-bond acceptor (HBA), hydrogen-bond donor (HBD), hydrophobic group (HY), and ring aromatic (RA) chemical feature types were selected to build the pharmacophore hypothesis. With respect to 15 kcal/mol energy threshold, a series of 255 conformers for each of the training compounds were used for chemical space sampling and pharmacophore model generation. Using the 3D QSAR protocol we generated top 10 hypotheses based on the 27 training compounds.

2.3. Pharmacophore model evaluation

A good QSAR model should be able to predict new compounds activities based on known ones. To ensure that our QSAR model can achieve the desired results, we performed a series of validation tests to assess the statistical robustness of the model [22,23].

2.3.1. Cost analysis

The DS software Catalyst allows evaluation of the generated hypothesis validity through the cost concept (estimated in bit units). Catalyst measure at first the cost in bit of an ideal hypothesis which is named fixed cost and represents the model that fits ideally all data. Then, the software estimates the cost of a null hypothesis named null cost which is the highest cost of a pharmacophore with no features. For each hypothesis a cost is calculated (total cost). As the difference between total cost and null cost increases, the probability of representing a true correlation of data by the model increases too. In general, a difference in cost more than 60 bits is considered as a good support to the validity of the model.

2.3.2. Fischer randomization

Fisher randomization method was used to evaluate the statistical significance of the selected Hypo1 hypothesis. Fisher's Validation method is based on generation of scrambled spreadsheets with randomly assigned activity to each compound. With the same parameters previously used for the unscrambled run, a new Hypo1 was generated for each random spreadsheet. To reach a confidence level of 95%, 19 random hypotheses were generated for comparison with the unscrambled run.

2.3.3. Decoy test

To assess a 3D pharmacophore model quality there are several useful enrichment descriptors [24]. Those metrics try to estimate the enrichment degree provided by a pharmacophore model to a chemical database. To benchmark our model we used the ZINC database to generate a chemical database of decoys for our 39 inhibitor using DecoyFinder tool v1.1 [25]. A database of 11,700 decoys has been produced according to some rules:

- Decoys and active compounds should have similar physical properties. This included the following physical descriptors: molecular weight, number of rotatable bonds, hydrogen bond donors, hydrogen bond acceptors and partition coefficient.
- Decoys have different chemical properties than active molecules. Using MACCS fingerprints decoys have been selected to have no more than 0.75 Tanimoto coefficient value with inhibitors.
- To achieve diversity and reduce incidence of analogous structures within the decoys subset, calculated Tanimoto coefficient between decoys structures should be no more than 0.9.

Some of the widely used metrics for VS successfulness is the enrichment factor (EF). EF calculate the fraction of retrieved active compounds in the top *x*% of a ranked list and compare it to the ratio between binders and decoys in the database.

$$EF^{x\%} = \frac{Hits^{x\%}(selected)/N^{x\%}(selected)}{Hits(total)/N(total)}$$

$Hits^{x\%}$ represents the number of hits at the top *x*% of database with N compound entries.

While the EF is widely used metrics for VS assessment, it suffers from the inability to distinguish between top ranked active molecules and lower scored actives. This leads to an equal contribution of active compounds in EF score without regard to their biological activity and rank in hit list.

Robust initial enhancement (RIE) is an advanced enrichment descriptor that was developed by Sheridan et al. to consider the ranking of compounds in the metrics [26].

The RIE descriptor relates the *i*th active compound to the number of scored compounds investigated *a*. *S* was calculated as following:

$$S = \sum_{i=1}^{actives} \exp(-rank(i)/a)$$

By the use of an exponential function, this method will allow the top active compound in the beginning of the hit list to mark the highest scores (*S*). The more we progress in the hit list the more *S* decreases. Then a random score $\langle S \rangle$ is assigned to randomly ranked active compounds and RIE was calculated as following:

$$RIE = \frac{S}{< S >}$$

This ensures comparison between a ranked list of actives found by a model and a random ranking. When RIE = 1 we have a random distribution of the active molecules. As RIE increases more than the value of 1, the performance of the screening model to retrieve active compounds in the beginning of the hit list increases too.

A better assessment of a pharmacophore model performance can be achieved using ROC curve.

ROC curve is plotted using the score of the top ranked active molecule as a threshold. Then the number of decoys within this cutoff is counted and corresponding sensitivity (Se) and specificity (Sp) values are calculated. This operation iterate through all active compounds in list until all score of active compounds were used as thresholds. By plotting the true positive rate (Se) versus the false positive rate (1 − Sp) we can represent the ROC curve. Using this curve we can also estimate the area under the curve (AUC). This measure can be calculated by summing surfaces of all rectangles formed for different thresholds. The used AUC formula was:

$$AUC = \sum_{i} [(Se_{i+1})(Sp_{i+1} - Sp_i)]$$

2.3.4. Leave one out method

To verify if any of the training compounds contributed more than the others in the pharmacophore generation we used the leave one out method. Using the same pharmacophore generation parameters we generated 27 top 10 hypotheses. Each time one compound was excluded from the set and a new model was created. This procedure was used to confirm reliability of the calculated correlation coefficients between experimental and predicted activity value. Another benefit of this procedure was to ensure that the generated model considered all compounds and was not dependant on a particular compound.

2.4. Ligand databases filtration

After the Hypo1 model validation, we used the pharmacophore as a query to search chemical databases for new potential ERK2 inhibitors. Five chemical databases have been screened using the pharmacophore query: ZINC database (5007), DrugBank (6558), Chembank (775,000), Maybridge (54,318) and NCI (750,690). All the databases have been subject to a filtration process to find drug-like properties. To avoid discarding molecules with possible inhibitory activity, known active molecules properties have been used to adjust filter range. Results showed that Lipinski rules should be relaxed to incorporate all the known active compounds. This enlarged filter was composed of (MW ≤ 550, HD ≤ 7, HA ≤ 10, and log *P* ≤ 6). Using Open Babel for databases filtration, the resulting compounds were: ZINC database (4127), DrugBank (1703), Chembank (151,949), Maybridge (42,809) and NCI (55,119). After that, we applied the Hypo1 pharmacophore query to the database in order to find active compounds fitting the selected rules. This mapping protocol produced 12,937 compounds fitting the Hypo1 pharmacophore model from 255,707 filtered compounds.

2.5. Molecular docking of ERK2

Docking was used in the focus of increasing the power of the results of the pharmacophore filter. Docking is useful in the workflow of the VS procedure because of its ability to search the conformational space of molecules. While pharmacophore filter ensure high speed of compound retrieval, it is limited by the inability to perfrom an exhaustive conformation search. Some compounds conformations may match the pharmacophore model but when analyzing, they are biologically irrelevant poses. Docking offers a solution to this issue by doing an exhaustive search for the most relevant conformation.

The Protein ERK2 was selected from RCSB Protein DataBank (PDB, www.rscb.org) PDB ID: 2OJJ.

ERK2 Protein was prepared by removing all water molecules and ligands. All the fitted compounds have been subject to a first round of docking to ERK2 Protein using the AUTODOCK Vina software [27]. Important parameters used in docking were default exhaustiveness value, a grid box centered in the ATP active site and a box seize of $29 \times 29 \times 18$ Å^3. During the docking process, the nine best conformations were saved for each ligand as a result of conformational space search. After a first round of docking, the best conformation of each compound has been chosen for a second round of docking. For this round we used an affinity cut off value of −5 kcal/mol. The resulting 1590 compounds were subject to a more exhaustive conformational search within the active site using a higher exhaustiveness parameter (exhaustiveness = 48). A final result of 54 compounds with predicted affinities values below −10 kcal/mol have been selected for further study. Analysis of the best compounds interaction with the ERK2 protein has been conducted using Discovery studios Visualizer 3.5.

2.6. Virtual counter screening

Drug selectivity is the ability of the drug molecule to target preferentially a particular protein, receptor or cell(s) than others. Protein kinases selectivity is known as a major problem in drug discovery [28,29]. This is partly due to the high degree of conservation inside the ATP catalytic site [30]. A basic way to deal with this issue can be by performing a counter screening of the selected hits against similar targets. Some possibly interfering targets with ERK2 ligands can be the following kinases: PKA, FLT3, SRC, LCK, GSK3, JNK, MEK1, P38a, KDR, CDK2, AURORA and ATK3. We have conducted 12 virtual counters screening docking using the top 54 molecules against ERK2 similar kinases. Target proteins have

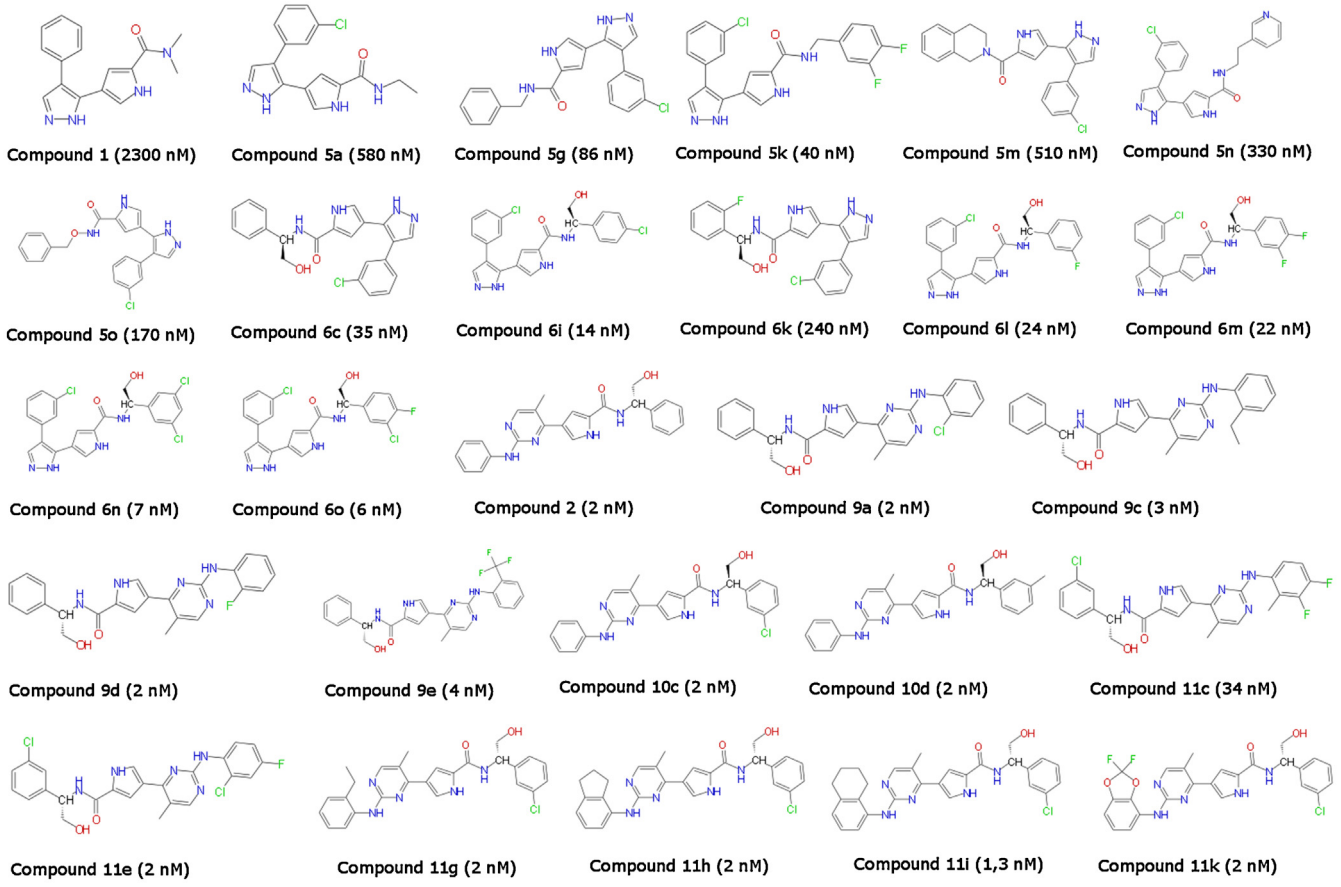

Fig. 1. The 27 chemically diverse compounds used as training set for the generation of the pharmacophore model. K_i nanomolar activities values are indicated for each compound.

been downloaded for RCSB PDB database and prepared for docking. Preparation phase included water molecules and ligands removal. ATP sites were identified and 3D coordinates of the catalytic site have been used for the docking by AUTODOCK VINA. Docked ligands have been ranked by affinity to kinases targets and values were compared to ERK2 affinity. Only hit molecules with predicted high affinity to ERK2 and low values to the other kinases have been retained.

To further profile the selectivity of our compounds we proceeded to hierarchical cluster analysis.

The clustering method is a statistical unsupervised method. It can insight about the natural organization of the data by arranging samples using similarity metrics. This approach helps finding similar patterns exhibited by a group of samples. Hierarchical clustering requires a metric as an input for samples distance measure. A linkage method is also needed in order to measure distance between two formed clusters.

Some of the common dissimilarity metrics are: Euclidean, Manhattan and Pearson correlation. Widely used linkage rules are: complete, single, average and ward. Using Euclidean distance and Ward linkage we performed a hierarchical clustering analysis on the counter screening matrix data.

2.7. Molecular dynamics simulation

Based on the docking results, molecular dynamics simulations were performed for the ERK2 protein with four ligands. Three of the ligands were issued from the top ten screened molecules and the fourth was the pyrazolylpyrrole ERK2 inhibitor. The Gromos force field was used with Gromacs 4.6.5, and ligand topology files were generated using the online PRODRUG server [31]. The protein was solvated with a-three centered water model in a periodic octahedronic box. Distance of at least 10 Å was respected between protein and the edge of the box. The systems were neutralized by adding sodium and chloride ions. Structures have been relaxed through 500 steps of steepest descent energy minimization. This was followed by respectively a 100 pico-seconds (ps) NVT, and 100 ps NPT equilibration phases. Solvation and equilibration phases were followed by a production of 10 ns. MD simulation was conducted with a time step of 2 femto-seconds (fs). Simulation physical conditions were temperature of 300 K and pressure of 1 bar. The modified Berendsen thermostat [32] and Parrinello-Rahman [33] were respectively used as thermostat and barostat coupling methods. Particle Mesh Ewald [34] method was used for long-range electrostatic interactions and the LINCS algorithm [35] was used to constrained all bonds. G_cluster allowed clustering of the last 5 ns of the equilibrated system. The first cluster was extracted and subject to minimization. Minimization involved relaxation through 400 steps of steepest descent followed by a 3000 steps of conjugate gradient energy minimization. The last frame was extracted for analysis. Hydrogen bonds module from Visual molecular dynamics 1.9.1 (VMD) was used for analysis of ligand-ERK2 hydrogen bonds. Discovery studios Visualizer 3.5 was also used for hydrogen and π interactions analysis.

3. Results and discussion

3.1. Pharmacophore model generation and examination

A training set of 27 compounds (Fig. 1) collected from literature have been used in this study for the generation of the

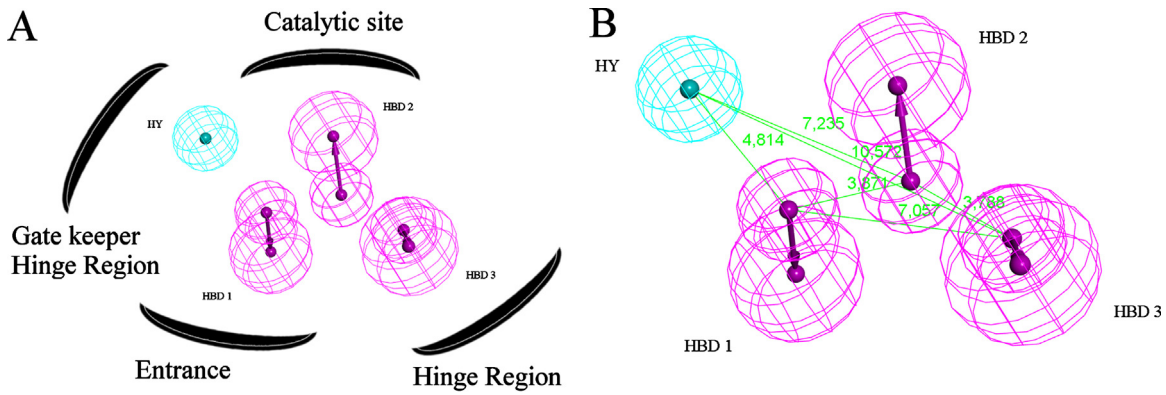

Fig. 2. The best Hypo1 pharmacophore model. (A) Chemical features of the Hypo1 model: hydrophobic (HY) in cyan and hydrogen bond donor (HBD) in magenta. Spatial arrangement of chemical features and their probable regions of interactions. (B) Features and their 3D spatial relationship; distances are in Angstrom.

Pharmacophore model. The discovery studio 2.5 3D QSAR Pharmacophore generation protocol was used to build the query model. Features used for the model building were hydrogen bond acceptor (HBA), hydrogen bond donor (HBD), hydrophobic (HY) and ring aromatic (RA). Based on the activity values of the training set, the ten best scored hypotheses were generated. Hypothesis1 (Hypo1) consisted of three HBD and one HY sites (Fig. 2). An analysis of the spatial arrangement of the chemical features in the ERK2 active site revealed their probable modes of interactions. HBD3 was in positions to interact with the hinge region containing Asp165 and Asn152. HBD2 pointed toward the catalytic site residue Lys52. HBD1 was in favorable position for engaging residues of the active site entrance. The HY feature was located toward the hinge region containing the gate keeper Gln103. All the pharmacophore features were located in favorable positions to engage important regions of the active site. Those preliminary findings suggest a good quality model. Moreover this Hypo1 pharmacophore model showed the highest cost difference (89,951), lowest error (94,431), best correlation coefficient (0,93), maximum fit value (7312) and lowest root mean square (RMS) of 1090. The fixed and the null cost values were respectively 99,367 and 205,404.

In our results, the majority of hypotheses contained HBD and HY groups suggesting an important role to play in the inhibition of the ERK2 kinase. We also noticed that our model was different from models created for P38a kinase. P38a models cited in later papers have in common hydrogen bond acceptor, hydrophobic and ring aromatic features [36,37]. This is not the case of our best model where there is no ring aromatic and hydrogen bond acceptor features. This may be because of the large training data sets used in those papers. However we think that the absence of shared features with P38a models can be an advantage in selecting a more ERK specific inhibitors.

Cost difference between null and fixed cost was more than 70 bits (89,951). All hypotheses showed correlation coefficient higher than 0.90. Hypo1 showed the best correlation coefficient values of 0.93 among all other hypotheses suggesting a good prediction capability of Hypo1. The fixed and total cost values of Hypo1 are respectively 99,367 and 115,453 and showed a very small difference (Table 1). Hypo1 showed the highest cost difference and correlation values with the lowest RMS and error values when compared to other hypotheses. Accordingly, Hypo1 was selected as the best hypothesis and used as a pharmacophore search query.

As one of the most potent inhibitors of the training set, Compound 10c (K_i = 2 nM) mapped well with the pharmacophore model. While the lesser potent compounds such as Compound 1 (K_i = 2300 nM) mapped features less precisely (Fig. 3).

Table 1
Top 10 hypothesis information and statistical significance as generated by Hypogen.

Hypothesis number	Total cost	Error cost	RMS	Correlation	Features
1	115.453	94.4315	1.09034	0.934699	HBD HBD HBD HY
2	116.989	95.2752	1.11863	0.931356	HBD HY R
3	118.141	97.1058	1.17768	0.923371	HBA HBA HBD HY
4	118.251	97.2504	1.18222	0.922747	HBD HY HY R
5	118.857	97.7165	1.19673	0.920782	HBD HBD HY R
6	118.891	97.6615	1.19503	0.921055	HBA HY HY R
7	119.586	98.5728	1.22295	0.917091	HBA HBD HBD
8	119.674	98.3236	1.21538	0.918214	HBA HBD HBD HY
9	119.966	97.8519	1.20092	0.920567	HBA HBD HY
10	120.07	98.4815	1.22018	0.917567	HBD HBD HY R

Null cost = 205.404; fixed cost = 99.3678; HBA = hydrogen bond acceptor; HBD = hydrogen bond donor; H = hydrophobic; RA = ring aromatic.

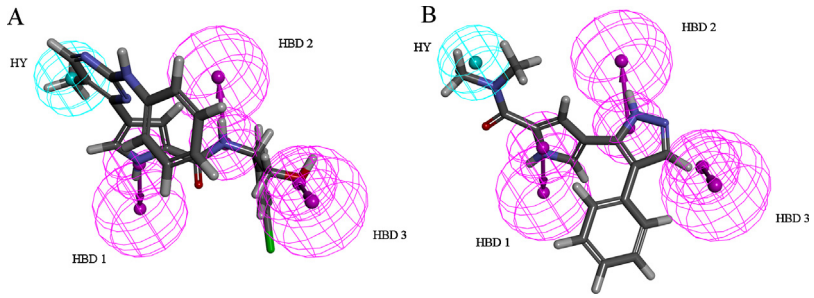

Fig. 3. Pharmacophore mapping. (A) Mapping of one of the most active molecules (compound 10c, K_i = 2 nM) on Hypo1. (B) Mapping of the least active molecule (compound 1, K_i = 2300 nM) on Hypo1.

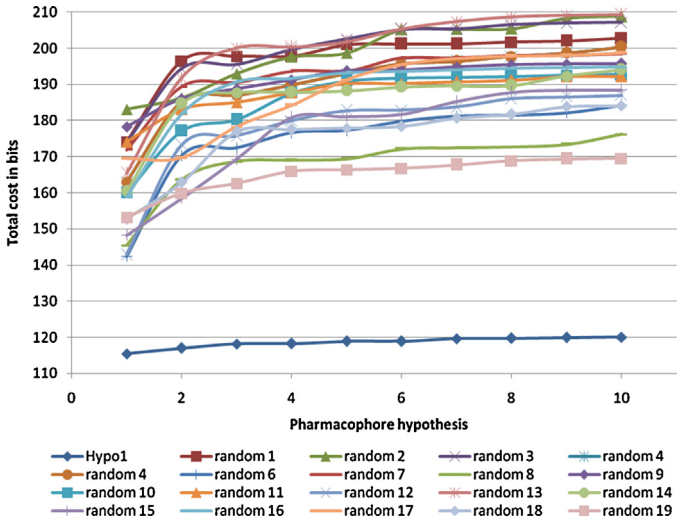

Fig. 4. Cost differences between Hypo1 and the 19 scrambled runs.

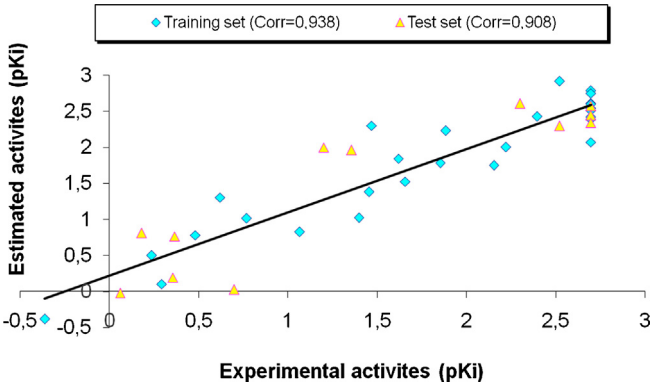

Fig. 5. Hypo1 prediction ability using linear regression. (A) Experimental versus Hypo1 estimated activities for the training set. (B) Experimental versus Hypo1 estimated activities for the test set.

Training set was subdivided into three groups based on activity values: highly active $K_i \leq 200$ nM = +++; moderately active $200 \leq K_i \leq 2000$ nM = ++ and inactive $K_i > 2000$ nM = + (Table 2).

3.2. Validation of hypo1

3.2.1. Method of Fischer randomization

To achieve a 95% confidence level, training set compounds have been reassigned random activities values and 10 new pharmacophore models were generated. This process was repeated 19 times to ensure the reliability of the hypothesis and to ensure that the generated hypothesis was not produced by chance. A good model should have lower cost bits than the randomly assigned activities models. This test showed clearly that Hypo1 hypothesis was statistically better than random models and thus was not generated by chance (Fig. 4).

3.2.2. Test set

Test set is used to check if the hypothesis is able to predict active compounds in sets other than in training one. The test set was prepared using the same method as the training. Compounds of the test set were classified into three categories based on their activity values: highly active $K_i \leq 200$ nM = +++; moderately active $200 \leq K_i \leq 2000$ nM = ++ and inactive $K_i > 2000$ nM = + With the exception of two compounds, all of the compounds activities were correctly estimated. Experimental and predicted activities of the test set according to Hypo1 are shown in (Table 3). A regression analysis graph plot of experimental activities versus estimated for both the training and test sets was drawn (Fig. 5). This clearly showed a good correlation of Hypo1 output with both the training (0.938) and test sets (0.908).

3.3. Decoy set

In order to further validate the discriminatory ability of the Hypo1 model, we generated 11700 decoy molecules using Decoyfinder and based on the ZINC drug-like database. Hypo1 was able to find 82% of active compounds in the hit list. At 1% of the database the model achieved a good enrichment factor of (74.35) and was able to find 29 compound from the 39 known actives (74.35%).

To estimate the contribution of the active molecules ranking in the enrichment, we calculated RIE. Value was $\gg 1$ indicating the superiority of the pharmacophore model ranking over random distribution.

Another good metrics to evaluate the performance of the pharmacophore model is the AUC of the ROC curve. Our model achieved a good value of 89% of AUC (Fig. 6).

4. Databases screening

Molecular properties of the training set ERK2 inhibitors suggest that Lipinski rules should be adjusted to allow the inclusion of compounds that proved to be active within a "relaxed" range of Lipinski rules. The suggested filter consisted of: ($MW \leq 550$, $HD \leq 7$, $HA \leq 10$, and $\log P \leq 6$). Finally we retained a total of 255707 compounds after applying the filter. Then we mapped the resulting database using the Hypo1 pharmacophore model. At last we retrieved 12,937 compounds fitting the Hypo1 pharmacophore model.

All mapped molecules have been subject to docking study into the ATP site of ERK2 protein.

4.1. Docking study

AutoDock Vina was used for the docking of ligands in the ATP active site of the ERK2 protein. For validation of Vina suitability to our study, we used two assessment methods.

First, we docked the original pyrazolylpyrrole ligand from PDB structure into the x-ray receptor structure. This showed an acceptable RMSD difference of 1.3 Å between X-ray and predicted structure (Fig. 7).

Secondly, we evaluated the performance of the docking tool to predict the correct activity value of the active compounds. Docking of the 39 active molecules into the ATP site of the ERK2 showed an acceptable correlation value of (0.69) between experimental and calculated K_i values. Based on the later results and the high speed capability of the AutoDock Vina tool, we decided to use it for the virtual screening procedure.

4.2. Virtual counter screening study

Because we targeted the ATP site of a kinase we expected that some of the found compounds will act promiscuously against other kinases. This behavior is a result of the evolutionary conservation of the ATP binding site among kinase proteins. Therefore we docked the top 1590 compounds against 12 kinase targets. The counter screen of the top 54 molecules results in 40

Table 2
The experimental and Hypo1 predicted K_i values of training set compounds.

Compound No.	Exp. K_i (μM)	Est. K_i (μM)	Error	Exp. activity scale	Est. activity scale
compound_9c	0.003	0.00121807	−2.46291	3+	3+
compound_10c	0.002	0.00163062	−1.22653	3+	3+
compound_10d	0.002	0.00177572	−1.1263	3+	3+
compound_2	0.002	0.00248186	1.24093	3+	3+
compound_9a	0.002	0.00249677	1.24839	3+	3+
compound_11e	0.002	0.00287203	1.43602	2+	3+
compound_9d	0.002	0.00307486	1.53743	2+	3+
compound_9e	0.004	0.00372579	−1.0736	3+	3+
compound_11k	0.002	0.00379187	1.89593	2+	3+
compound_11g	0.002	0.00407582	2.03791	2+	3+
compound_11c	0.034	0.00501701	−6.77694	3+	3+
compound_11i	0.013	0.00584001	−2.22602	3+	3+
compound_11h	0.002	0.00849934	4.24967	3+	3+
compound_6o	0.006	0.00999492	1.66582	3+	3+
compound_6l	0.024	0.0143785	−1.66916	3+	3+
compound_6i	0.014	0.0166106	1.18647	3+	3+
compound_6n	0.007	0.0177626	2.53751	3+	3+
compound_6m	0.022	0.0299043	1.35929	3+	3+
compound_6c	0.035	0.0414557	1.18445	3+	3+
compound_6k	0.24	0.0496936	−4.8296	2+	3+
compound_5k	0.04	0.0950805	2.37701	3+	3+
compound_5o	0.17	0.0970901	−1.75095	3+	3+
compound_5g	0.086	0.148334	1.72481	3+	3+
compound_5n	0.33	0.165104	−1.99874	2+	3+
compound_5a	0.58	0.316589	−1.83203	2+	2+
compound_5m	0.51	0.786111	1.54139	2+	2+
compound_1	2.3	2.41717	1.05094	1+	1+

compounds with high specificity to ERK2. The pyrazolylpyrrole ligand bound to X-ray ERK2 ATP site has been ranked the 30th compound of the top 54. As in vitro experiments [15,16], the docked pyrazolylpyrrole compound expressed high specificity profile toward ERK2.

To test specificity of our compounds toward ERK2, we docked a total number of 1590 compound against eleven kinases. Used kinases were KDR, FLT3, GSK3, SRC, JNK3, CDK2, AURORA, P38A, MEK1, ATK3, LCK and PKA. We conducted analysis based on calculated K_i from free energy of binding. Formula used in conversion was: $\Delta G = RT \ln(K_i)$ where $R = 1.986 \times 10^{-3}$ kcal/mol, $T = 298$ K and K_i in nanomolar. 942 (59.2%) compound docked into ERK2 kinase had a calculated $K_i < 1$ μM. Selected inhibition activity threshold was set at 20 nM. Our analysis showed that every kinase was docked by at least one compound with affinity under the 20 nM. We got a total of 93 (5.8%) compounds under the activity threshold of 20 nM. 29 (1.8%) of them docked within the range of selected affinity to only one single kinase. From the highly selective 29 compounds, 4 compounds originated from CHEMBANK (ID: 2099652, 3010993, 640629, and 1942588) docked selectively into ERK2.

Using docking affinity values we setup a matrix table for all screened kinases. To rank kinases selectivity we used the selectivity score $S(x)$ [38]. S is the number of kinases bound by an inhibitor with an affinity greater than "x" micromole divided by the number of tested kinases. Although the threshold value is the major criticism of this method, it can help ranking kinases by their selectivity toward compounds. Using the same principle we calculated an inhibition score $I(x)$ for each compound. "I" represents the number of compounds bound to a kinase with a selected affinity threshold, divided by the number of tested compounds. The inhibition score helped us identify compounds that bind to multiple kinases within affinity range. With aid of scores we found that ERK2, PKA, LCK and AKT3 scored the best affinity values. They also docked the largest number of tested compounds. On the other side, KDR, FLT2 and GSK kinases got the lowest scores and thus were very selective toward compounds. Analysis of the virtual counter screening of the 1590 molecule showed that PKA, ERK2 and LCK bound respectively with 66, 54 and 38 compounds below 20 nM barrier. Analysis of the top 54 compounds with affinity better than −10 kcal/mol showed that ERK2 ranked first before PKA. We also noticed that the largest number of ERK2 selective inhibitors was located below the −10 kcal/mol affinity threshold. This finding was expected since the training data set of the pharmacophore model expressed mean docking value of −9.9 kcal/mol ± 0.5.

Table 3
The experimental and Hypo1 predicted K_i values of test set compounds.

Compound No.	Exp. K_i (μM)	Est. K_i (μM)	Exp. activity scale	Est. activity scale
compound 11f	0.005	0.00245877	3+	3+
compound 11j	0.002	0.00265699	3+	3+
compound 11b	0.002	0.00358661	3+	3+
compound 9b	0.002	0.0045488	3+	3+
compound 11m	0.003	0.00504499	3+	3+
compound 6h	0.063	0.0100444	3+	3+
compound 6j	0.044	0.0109403	3+	3+
compound 6b	0.66	0.154281	2+	3+
compound 5d	0.43	0.171383	2+	3+
compound 5j	0.44	0.641913	2+	2+
compound 5b	0.2	0.940818	2+	2+
compound 5c	0.87	1.04884	2+	2+

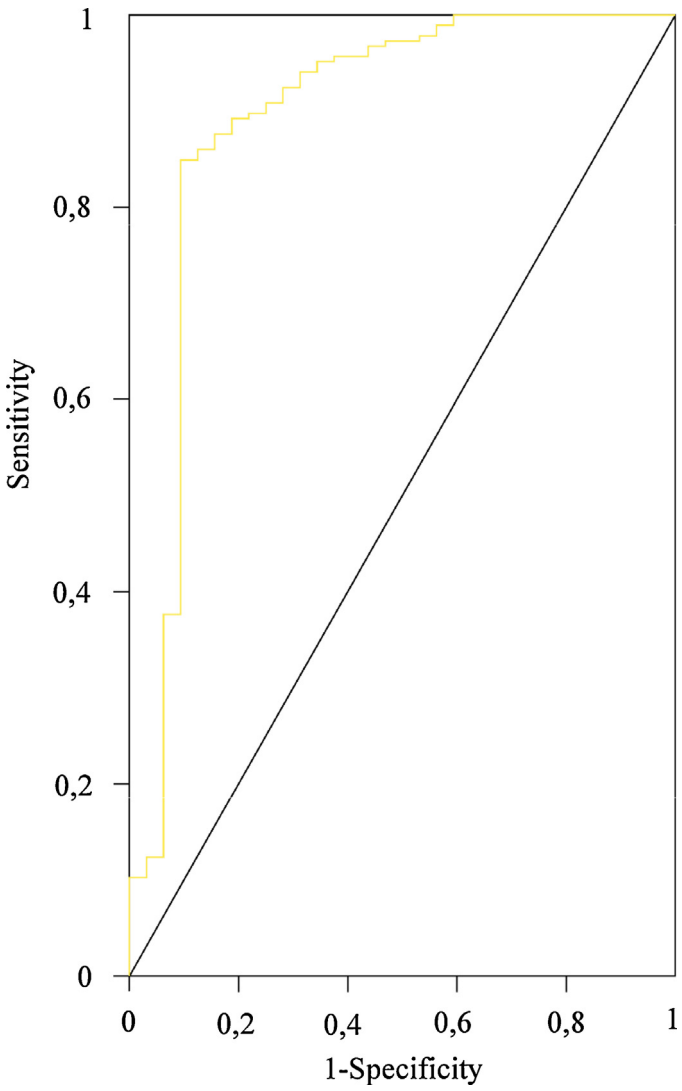

Fig. 6. ROC curve obtained by Hypo1 against randomly curve in the database screening.

To identify the most potent and selective ERK2 inhibitors, we used the docking data to perform a hierarchical cluster analysis. The result showed that our kinases can be separated into four large clusters according to their binding profiles. The first cluster contained only ERK2 kinase which has the highest affinity scores and the largest number of docked compounds. LCK, PKA and AKT3 were in the second cluster and they expressed similar binding behavior toward our virtual screening compounds. The third cluster of kinases was composed of MEK1, AURORA, SRC, CDK2, JNK3 and P38A. Finally KDR, FLT2 and GSK proteins populated the fourth group and exhibited low binding profile toward compounds. This later group also scored the lowest inhibitory $I(x)$ values in agreement with hierarchical clustering.

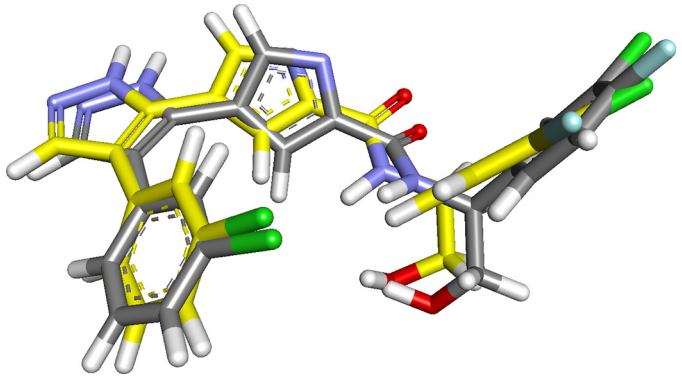

Fig. 7. Superimposition of X-ray pyrazolylpyrrole derived compound (carbons in yellow) and Vina predicted one (carbons in gray).

In order to pick the most selective ERK2 compounds we performed compounds clustering. Results indicate that docked compounds can be arranged into three groups according to the docking energies: high, moderate and low affinity. On the top of the heat map, the first cluster contains the most promiscuous compounds. Except for KDR, the members of this compound cluster docked to almost all kinases with high affinity. On the bottom of the heatmap we have found 285 docked compounds with very low affinities to all of the 13 targets. In the middle of the heatmap, cluster analysis identified the cluster number 2 where we did find a number of interesting compounds. In this group, a sub cluster of 261 compounds was formed by molecules with high selectivity toward ERK2.

Among those compounds we have found all the 54 Vina top ranked compounds. Further analysis of the 261 molecules showed that 6 of them (Compounds ID 2117128, 1886675, 3187613, RRS, 1886900 and 3130761) (Fig. 8) were predicted to exhibit very selective binding profile toward ERK2. All the 6 molecules were parts of the top 54 compounds ranked by docking and they scored the lowest $S(x)$ and $I(x)$ values. Those results highlighted the importance of the pharmacophore model and its capability to enhance the selectivity ratio in a compound database.

A comparison of clusters showed that cluster number 2 compounds were the most selective toward ERK2 when they are in the range of 20–50 nM. With lower than 20 nM of predicted K_i, our ERK2 selectivity decrease and some compounds are predicted to bind with PKA too (Fig. 9).

4.3. Analysis of protein–ligand complexes

We used AutoDock Vina to perform docking of the pyrazolylpyrrole compound 82A and study its binding modes for further docking comparison. Our docking results are in agreement with the binding mode of X-ray active compound.

The ligand structures with the best affinity energy to the ERK2 ATP site were selected for analysis (Table 4).

Analysis of the best scored poses showed that interaction between compounds and ERK2 ATP site can follow certain modes. Some compounds interact with the hinge region of the receptor mainly by establishing hydrogen bonds with Asp165 and Asn152. The glycine rich loop was found to be frequently involved in binding tightly the compounds through not only hydrogen bonds but also Pi interactions. This was the case of compounds 1886675 and 3130761. The majority of compounds engaged the catalytically important residue Lys52 through hydrogen bonds. An exception of the hydrogen bonding with Lys52 was represented by Compound 188690 which involved its indoline group in a Pi–Pi interaction mode. Hinge region containing the gate keeper Gln103 was also another site involved in binding ERK2 predicted inhibitors. Binding modes involving this region were mainly hydrogen bonds. Interaction of compounds with the gate keeper region was less frequent than with other sites of the ATP pocket. The compound 3187613 was successful in binding the gatekeeper region through oxygen's linked to the tetrahydropyran ring. Another mode of binding compounds into the ERK2 active site was through hydrogen bonds with residues in the entrance of the ATP pocket. This was the case of Compound 1886675 that engaged the sp2 oxygen of the methylethanolamine group and the nitrogen atom of the cyclotetradecane group in respective hydrogen interactions with Lys112

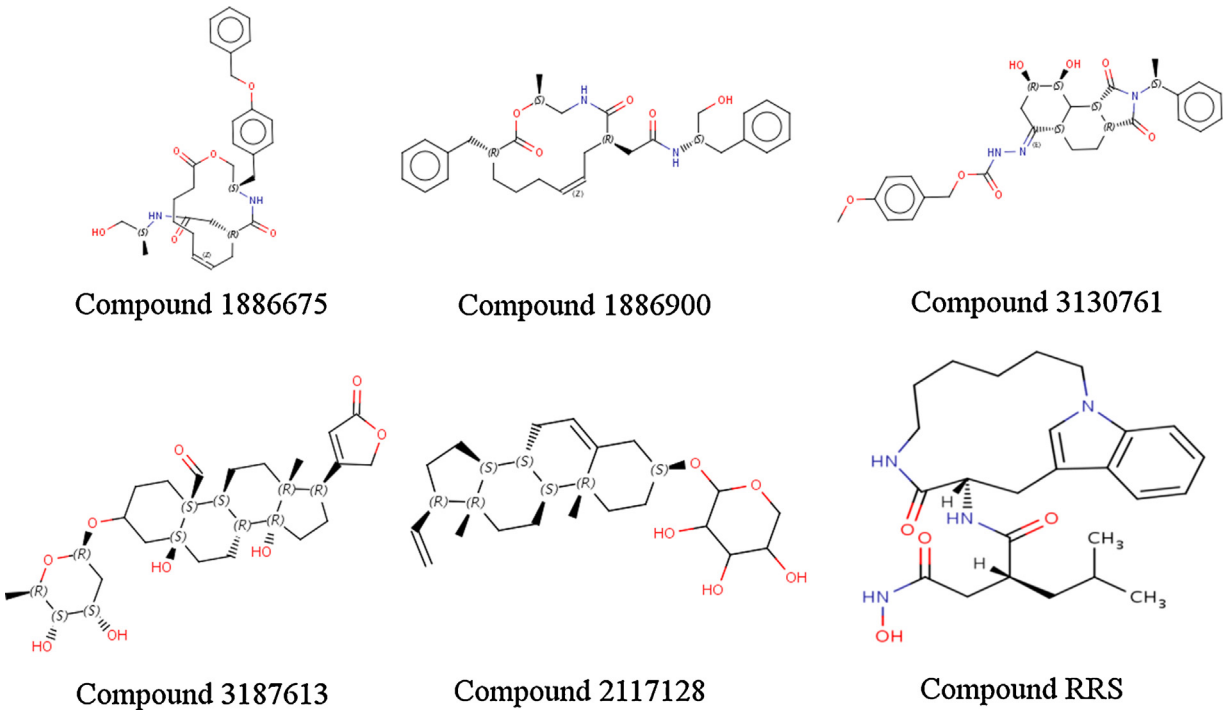

Fig. 8. The highly scored ERK2 inhibitors as predicted by affinity values of Autodock Vina.

and Ser151. Our analysis helped further decompose the ERK2 active site into functional regions where interaction is crucial to inhibit the kinase activity. Five site of interaction within the ATP site are the most important in the expression of an inhibitory activity. They are the flexible glycine rich loop, the hinge region containing Asp165 and Asn152, the hinge region containing the gatekeeper Gln103, the important catalytic site containing Lys52 and the site entrance residues.

Our analysis results showed also that compound interaction modes with ERK2 active sites were similar to the modes discovered in X-ray.

The docked 82A compound engaged hydrogen bonds with Tyr34, Lys52 (the catalytic site), Gln103 (the gate keeper), Asp104, Met106 (hinge region), and Asp165 (the salt bridge area). Those hydrogen interactions were responsible for the experimental high inhibitory activity and selectivity toward ERK2 (Fig. 10).

Docking analysis showed that almost all predicted selective compounds involved the glycine rich loop and/or the catalytic site. This was predictable since inhibiting the catalytic site will probably lead to decrease in the overall kinase activity. Moreover it is known that the glycine rich loop can be the drive of both potency and selectivity and thus it form an important region to consider during a rational drug design projects [39–41]. Accordingly we think that this combination can be probably important in expressing an inhibitory activity with the highest possible selectivity.

4.4. Molecular dynamics study

Proteins in physiological conditions are not static but dynamic macromolecules interacting in their medium generally composed of water. This dynamics process can affect both the structure of the protein and its relation with its environment especially ligands. In view of this, we used MD simulation to assess stability of the ligand–protein complex.

We run 10 ns MD for the Pyrazolylpyrrole based compound to assess stability of the ligand–protein complex. We also analyzed a 10 ns MD for 2 of the predicted most selective compounds (2117128, 3187613).

RMSD of each ligand-ERK2 complex has been outlined in the Fig. 11. Our analysis showed that ERK2 receptor and its respective ligands showed a mean RMSD value of 1.86 ± 0.21 Å for the backbone and 0.85 ± 0.2 Å for the ligands. All three protein–ligand trajectories showed stable and low RMSD values, indicating stable complexes during simulation.

Hydrogen bonds have been analyzed over the last 5 ns of each simulation when all systems showed the most stable RMSD values.

MD Analysis of the pyrazolylpyrrole ligand interaction with ERK2 showed that the ligand conserved its hydrogen bond with Lys52. We noticed also that hydrogen bonds involving Gln103 (distance increased from 1.3 Å to 5.2 ± 0.7 Å) and Asp104 have broken by torsion of the nitrogenated bi-cyclopentyl (by 33°). Furthermore, the ligand 2-fluorotoluene group has been subject to 2.32 Å

Table 4
Summary of predicted selective compounds and their interaction modes with ERK2 ATP site.

Compound	HB	Pi–Pi	Pi_cation	Hinge region	Glycine rich loop	Catalytic site	Hinge region	Active site entrance residues
2117128	Tyr34, Gly35, Lys52, Asp165			+	+	+		
1886675	Glu31, Ala33, Tyr34, Gly35, Lys52, Lys112, Ser151	Tyr34	Lys52		+	+		+
3187613	Ser151, Asp109, Ala33, Tyr34, Gly35, Met106				+		+	+
RRS	Glu31, Lys52, Glu69, Gln103		Arg65	+	+	+		
1886900			Lys52		+	+		
3130761	Asn152	Tyr34			+	+		+

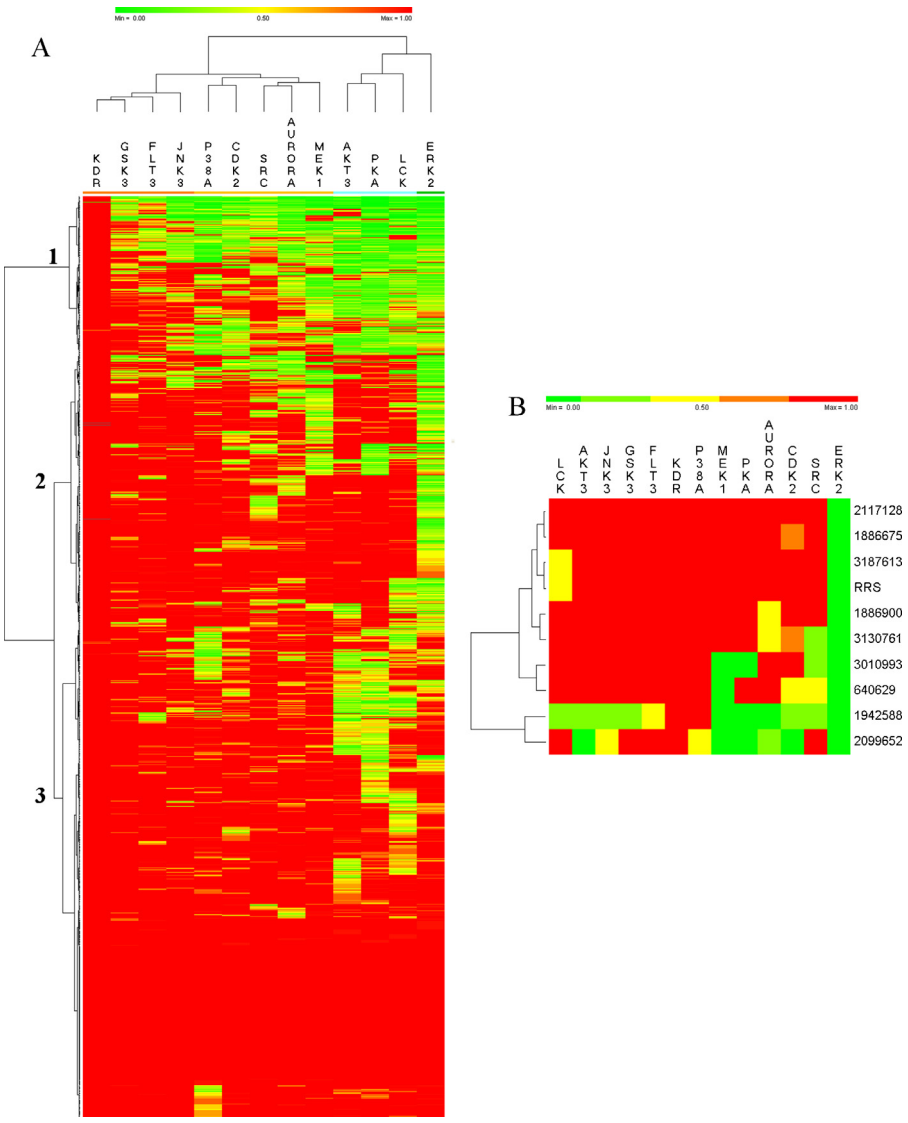

Fig. 9. Hierarchical cluster analysis of virtual counter screening affinities. (A) 1590 compound profiled against 13 kinases. (B) Affinity profile of the most ERK2 selective compounds.

translation and 23° torsion leading to the formation of a new hydrogen bond with Gly32 (Fig. 10A and B) (Fig. 12A). No π interaction can be detected between ligand and its active site during the 10 ns of the simulation confirming the finding of the docking results.

Analysis of the three MD results suggested stability of the ligands into their respective active sites. We also noticed that during simulation studied compounds maintained almost the same modes of interactions predicted by docking. MD confirmed that involved ERK2 regions in binding inhibitors where catalytic site (Lys52), Glycine rich loop, Hinge region (Asp165), Gatekeeper region (Gln103, Met106) and ATP site entrance residues (Ser151). MD confirmed docking results of both stability of the ERK2-ligand complex and the presumed active conformation.

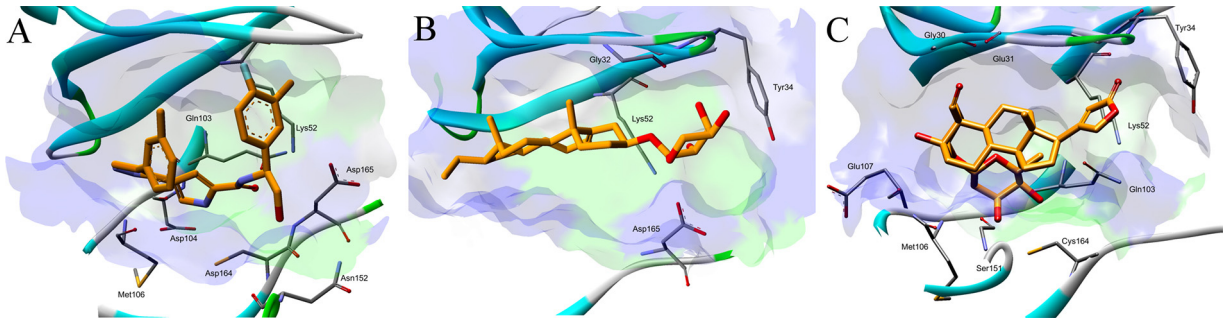

Fig. 10. Close view of amino acids involved in binding compounds into ERK2 ATP site. (A) Pyrazolylpyrrole compound. (B) Compound ID 2117128 and (C) Compound ID 3187613.

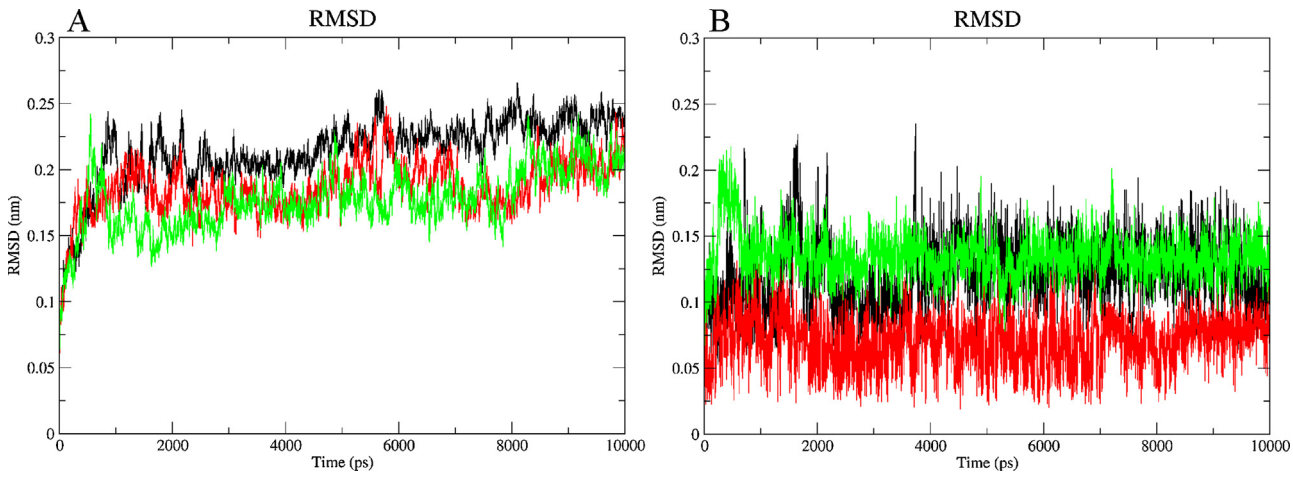

Fig. 11. (A) RMSD profile for backbone atoms of the ERK2 protein. (B) RMSD profile for ERK2 ligands. In black: ERK2 protein with compound pyrazolylpyrrole. In red: compound ID 2117128 In green: compound ID 3187613.

Finally, using a set of known active ERK2 inhibitors we generated a pharmacophore model able to find active compounds. Molecules resulting from pharmacophore mapping have been subject to docking into the ERK2 receptor. To minimize the kinase specificity problem we did performed a virtual counter screening involving a number of kinases. The resulting compounds were subject to stability analysis using molecular docking.

5. Conclusion

The purpose of this study was to build a pharmacophore model able to predict ERK2 protein inhibitory activity. This was through exploring multiple compound databases for new molecules scaffolds able to guide further studies concerning ERK2 specific inhibition. In this work, we have generated 3D pharmacophore model from a training set of 27 known ERK inhibitors. Correlation coefficient of the best scored model with both training and test set were 0.938 and 0.908 respectively, suggesting reliable predictability value. The best scored pharmacophore model has been used as 3D query for screening large compound databases like ZINC, NCI, Chembank and Drugbank. All compounds resulting from the fitting step have been subject to docking using AutDock Vina. A virtual counter screening process helped us choosing the best selective ERK2 compounds. Finally, a docking/MD analysis were conducted to identify the modes of binding and the most important regions of the ATP site. MD confirmed the docking results and the modes of binding. Hydrogen bonds have been identified between studied compounds and five important region of the ERK active site. Catalytic site (Lys52), Glycine rich loop, Hinge region (Asp165), Gatekeeper region (Gln103, Met106) and ATP site entrance residues (Ser151) represents important regions to target. We also noticed that catalytic site and glycine rich loop were the driver for high potency inhibition and better selectivity. Finally, this study was provided in order to address the problem of finding new compounds/scaffold with high potency and selectivity against ERK2 and serve as a starting point for lead optimization and scaffold hopping.

Appendix A. Supplementary data

Supplementary material related to this article can be found, in the online version, at http://dx.doi.org/10.1016/j.jmgm.2014.07.001.

References

[1] P. Cohen, Protein kinases – the major drug targets of the twenty-first century? Nat. Rev. Drug Discov. 1 (4) (2002) 309–315.
[2] T. Ravingerová, M. Barancík, M. Strnisková, Mitogen-activated protein kinases: a new therapeutic target in cardiac pathology, Mol. Cell Biochem. 247 (1-2) (2003) 127–138.
[3] K. Imahori, T. Uchida, Physiology and pathology of tau protein kinases in relation to Alzheimer's disease, J. Biochem. 121 (2) (1997) 179–188.
[4] Y. Feng, J. Wen, C.C. Chang, p38 mitogen-activated protein kinase and hematologic malignancies, Arch. Pathol. Lab Med. 133 (11) (2009) 1850–1856.
[5] M. Towatari, H. Iida, M. Tanimoto, H. Iwata, M. Hamaguchi, H. Saito, Constitutive activation of mitogen-activated protein kinase pathway in acute leukemia cells, Leukemia 11 (4) (1997) 479–484.
[6] P.J. Roberts, C.J. Der, Targeting the Raf-MEK-ERK mitogen-activated protein kinase cascade for the treatment of cancer, Oncogene 26 (22) (2007) 3291–3310.
[7] S. Banerjee, S.B. Kaye, New strategies in the treatment of ovarian cancer: current clinical perspectives and future potential, Clin. Cancer Res. 19 (5) (2013) 961–968.
[8] D. Datta, A.G. Contreras, A. Basu, O. Dormond, E. Flynn, D.M. Briscoe, S. Pal, Calcineurin inhibitors activate the proto-oncogene RAS and promote pro-tumorogenic signals in renal cancer cells, Cancer Res. 69 (23) (2009) 8902–8909.
[9] C. Song, W. Wang, M. Li, Y. Liu, D. Zheng, Tax1 enhances cancer cell proliferation via Ras-Raf-MEK-ERK signaling pathway, IUBMB Life 61 (6) (2009) 685–692.
[10] E.A. Collisson, C.L. Trejo, J.M. Silva, S. Gu, J.E. Korkola, L.M. Heiser, R.P. Charles, B.A. Rabinovich, B. Hann, D. Dankort, P.T. Spellman, W.A. Phillips, J.W. Gray, M. McMahon, Central role for RAF→MEK→ERK signaling in the genesis of pancreatic ductal adenocarcinoma, Cancer Discov. 2 (8) (2012) 685–693.
[11] J.R. Sierra, V. Cepero, S. Giordano, Molecular mechanisms of acquired resistance to tyrosine kinase targeted therapy, Mol Cancer. 9 (2010) 75.
[12] J.A. McCubrey, L.S. Steelman, S.L. Abrams, F.E. Bertrand, D.E. Ludwig, J. Bäsecke, M. Libra, F. Stivala, M. Milella, A. Tafuri, P. Lunghi, A. Bonati, A.M. Martelli, Targeting survival cascades induced by activation of Ras/Raf/MEK/ERK, PI3K/PTEN/Akt/mTOR and Jak/STAT pathways for effective leukemia therapy, Leukemia 22 (4) (2008) 708–722.
[13] R. Srinivasan, T. Zabuawala, H. Huang, J. Zhang, P. Gulati, S. Fernandez, J.C. Karlo, G.E. Landreth, G. Leone, M.C. Ostrowski, Erk1andErk2 regulate endothelial cell proliferation and migration during mouse embryoangiogenesis, PLoS One 4 (12) (2009) e8283.
[14] C.N. Prowse, J. Lew, Mechanism of activation of ERK2 by dual phosphorylation, J. Biol. Chem. 276 (1) (2001) 99–103.
[15] A.M. Aronov, C. Baker, G.W. Bemis, J. Cao, G. Chen, P.J. Ford, U.A. Germann, J. Green, M.R. Hale, M. Jacobs, J.W. Janetka, F. Maltais, G. Martinez-Botella, M.N. Namchuk, J. Straub, Q. Tang, X. Xie, Flipped out: structure-guided design of selective pyrazolylpyrrole ERK inhibitors, J. Med. Chem. 50 (6) (2007) 1280–1287.
[16] Aronov AM1, Q. Tang, G. Martinez-Botella, G.W. Bemis, J. Cao, G. Chen, N.P. Ewing, P.J. Ford, U.A. Germann, J. Green, M.R. Hale, M. Jacobs, J.W. Janetka, F. Maltais, W. Markland, M.N. Namchuk, S. Nanthakumar, S. Poondru, J. Straub, E. ter Haar, X. Xie, Structure-guided design of potent and selective pyrimidylpyrrole inhibitors of extracellular signal-regulated kinase (ERK) using conformational control, J. Med. Chem. 52 (October (20)) (2009) 6362–6368.
[17] G. Wolber, T. Langer, LigandScout: 3-D pharmacophores derived from protein-bound ligands and their use as virtual screening filters, J. Chem. Inf. Model 45 (1) (2005) 160–169.

[18] M.L. Peach, M.C. Nicklaus, Combining docking with pharmacophore filtering for improved virtual screening, J. Cheminform. 1 (1) (2009) 6.
[19] Chen Z1, H.L. Li, Q.J. Zhang, X.G. Bao, K.Q. Yu, X.M. Luo, W.L. Zhu, H.L. Jiang, Pharmacophore-based virtual screening versus docking-based virtual screening: a benchmark comparison against eight targets, Acta Pharmacol. Sin. 30 (12) (2009) 1694–1708.
[20] L.B. Kier, Molecular orbital calculation of preferred conformations of acetylcholine, muscarine, and muscarone, Mol. Pharmacol. 3 (5) (1967) 487–494.
[21] L.B. Kier, MO Theory in Drug Research, Academic Press, New York, 1971, pp. 164–169.
[22] R.C. Braga, C.H. Andrade, Assessing the performance of 3D pharmacophore models in virtual screening: how good are they? Curr. Top. Med. Chem. 13 (9) (2013) 1127–1138.
[23] S.Y. Yang, Pharmacophore modeling and applications in drug discovery: challenges and recent advances, Drug Discov. Today 15 (June (11–12)) (2010) 444–450.
[24] Kirchmair J1, P. Markt, S. Distinto, G. Wolber, T. Langer, Evaluation of the performance of 3D virtual screening protocols: RMSD comparisons, enrichment assessments, and decoy selection—what can we learn from earlier mistakes? J. Comput. Aided Mol. Des. 22 (March–April (3–4)) (2008) 213–228.
[25] A1 Cereto-Massagué, L. Guasch, C. Valls, M. Mulero, G. Pujadas, S. Garcia-Vallvé, DecoyFinder: an easy-to-use python GUI application for building target-specific decoy sets, Bioinformatics 28 (June (12)) (2012) 1661–1662.
[26] R.P1 Sheridan, S.B. Singh, E.M. Fluder, S.K. Kearsley, Protocols for bridging the peptide to nonpeptide gap in topological similarity searches, J. Chem. Inf. Comput. Sci. 41 (September-October (5)) (2001) 1395–1406.
[27] O. Trott, A.J. Olson, AutoDock Vina: improving the speed and accuracy of docking with a new scoring function, efficient optimization and multithreading, J. Comput. Chem. 45 (2010) 5–461.
[28] M.A. Fabian, W.H. Biggs III, D.K. Treiber, C.E. Atteridge, M.D. Azimioara, M.G. Benedetti, T.A. Carter, P. Ciceri, P.T. Edeen, M. Floyd, J.M. Ford, M. Galvin, J.L. Gerlach, R.M. Grotzfeld, S. Herrgard, D.E. Insko, M.A. Insko, A.G. Lai, J.M. Lélias, S.A. Mehta, Z.V. Milanov, A.M. Velasco, L.M. Wodicka, H.K. Patel, P.P. Zarrinkar, D.J. Lockhart, A small molecule-kinase interaction map for clinical kinase inhibitors, Nat. Biotechnol. 23 (3) (2005) 329–336.
[29] Karaman MW1, S. Herrgard, D.K. Treiber, P. Gallant, C.E. Atteridge, B.T. Campbell, K.W. Chan, P. Ciceri, M.I. Davis, P.T. Edeen, R. Faraoni, M. Floyd, J.P. Hunt, D.J. Lockhart, Z.V. Milanov, M.J. Morrison, G. Pallares, H.K. Patel, S. Pritchard, L.M. Wodicka, P.P. Zarrinkar, A quantitative analysis of kinase inhibitor selectivity, Nat. Biotechnol. 26 (January (1)) (2008) 127–132.
[30] Yuliet Mazola, Rolando Rodriguez, Protein kinases as targets for drug design, Biotecnologia Aplicada 25 (2008) 7–15.
[31] A.W. Schüttelkopf, D.M. van Aalten, PRODRG: a tool for high-throughput crystallography of protein-ligand complexes, Acta Crystallogr. D: Biol. Crystallogr. 60 (Pt 8) (2004) 1355–1363.
[32] P.H. Hünenberger, Thermostat algorithms for molecular dynamics simulations, Adv. Polym. Sci. 173 (2005) 105–149.
[33] N. Shuichi, M.L. Kleina, Constant pressure molecular dynamics for molecular systems, Mol. Phys. 50 (1983) 1055–1076.
[34] U. Essmann, L. Perera, M.L. Berkowit, T. Darden, H. Lee, L.G. Pedersen, A smooth particle mesh Ewald method, J. Chem. Phys. 103 (19) (1995) 8577–8593.
[35] H. Berk, B. Henk, H.J.C. Berendsen, J.G.E.M.L.I.N.C.S. Fraaije, A linear constraint solver for molecular simulations, J. Comput. Chem. 18 (12) (1997) 1463–1472.
[36] R. Sarma, S. Sinha, M. Ravikumar, M. Kishore Kumar, S.K. Mahmood, Pharmacophore modeling of diverse classes of p38 MAP kinase inhibitors, Eur. J. Med. Chem. 43 (12) (2008) 2870–2876.
[37] K. Gugan, M. Thirumurthy, G. Changdev, J. Seung, A combined 3D QSAR and pharmacophore-based virtual screening for the identification of potent p38 MAP kinase inhibitors: an in silico approach, Med. Chem. Res. 22 (2013) 1773–1787.
[38] T. Anastassiadis, S.W. Deacon, K. Devarajan, H. Ma, J.R. Peterson, Comprehensive assay of kinase catalytic activity reveals features of kinase inhibitor selectivity, Nat. Biotechnol. 29 (October (11)) (2011) 1039–1045.
[39] D. Toader, A.D. Ferguson, Structural approaches to obtain kinase selectivity, Trends Pharmacol. Sci. 33 (5) (2012) 273–278.
[40] Huse M1, J. Kuriyan, The conformational plasticity of protein kinases, Cell 109 (3) (2002) 275–282.
[41] L.N. Johnson, M.E. Noble, D.J. Owen, Active and inactive protein kinases: structural basis for regulation, Cell 85 (April (2)) (1996) 149–158.